International Journal of Heat and Mass Transfer 51 (2008) 5851–5858

Contents lists available at ScienceDirect

International Journal of Heat and Mass Transfer

journal homepage: www.elsevier.com/locate/ijhmt

An application of infinite regular polyhedrons geometry to design heat exchangers

Miroslaw Zukowski *

Department of Heat Engineering, Bialystok Technical University, Wiejska 45 A, 15-351 Bialystok, Poland

ARTICLE INFO

Article history:
Received 15 January 2008
Received in revised form 15 April 2008
Available online 2 July 2008

Keywords:
Heat exchanger
Heat and mass transfer
Pressure drop
CFD
Numerical simulation
Infinite regular polyhedrons

ABSTRACT

Paper presents an idea of utilization infinite regular polyhedrons for designing heat exchange devices. The investigated prototype of the heat exchanger was consisted of twenty identical solids. Each of them was composed from eight regular hexagons. CFD simulations, reported in this paper, were used to obtain an influence of the flow domain modification on the intensification of the forced convection heat transfer in the developed device. Computational analyses clearly showed that the experimental testing of the heat exchanger prototype should be realized with include of cuboid turbulence inserts. Heat transfer performance and pressure drop obtained by experimental investigations are presented, too. The average Nusselt number and Fanning friction factor were expressed in terms of the Reynolds number.

1. Introduction

One of the problems, that solid geometry solves lie in complete fill any space with identical Archimedes or Platon polyhedrons. The final solid is constructed by moving a base element parallel to axis of Cartesian coordinate system. The author proposes using the geometry of infinite regular polyhedrons for designing heat exchange devices. There are three types of solids filling the space in the form of two congruent labyrinths. The basic structural component of the first solid consists of squares. As shown in Fig. 1, six of them have a common vertex. The second solid, which is presented in Fig. 2, has four hexagons with a common vertex. In the third case (Fig. 3), six hexagons meet in the common vertex.

All regular polyhedrons, presented here, can be applied in a wild verity of engineering applications as parallel, cross and counter flow heat exchangers. Furthermore, it is possible to design short term thermal energy storage (TES) unites based on the referred solids. In this variant of construction, phase change material (PCM) should fill out one of labyrinths.

The available literature review shows that there are no reports of selected geometry among the heat transfer applications. Only some projects are loosely related to investigated heat exchanger.

Lu used analytical models to evaluate the efficiency of microcell aluminum honeycombs heat exchanger. The fluid flow in a honeycomb core was laminar. In Ref. [1] author reported that the optimal cell morphology is not constant but depend upon the geometry and heat transfer condition. It was concluded that the optimal relative density of the honeycombs is about 0.1. Construction geometry tested by Lu is illustrated in Fig. 4.

In Ref. [2] laminar and fully developed flow trough single- and double-trapezoidal ducts using a finite-difference method were only theoretically analyzed by Sadasivam, Manglik and Jog. Fig. 5 shows the geometry of investigated heat exchanger. Simulations of velocity and temperature fields were obtained for a wide range of duct aspect ratios and with four different trapezoidal angles. The influence of a duct aspect ratio on *Re* number and *Nu* number was presented in the form of polynomials. A strong dependence of thermal and pressure drop characteristics on duct geometry was reported.

Yeh et al. [3] experimentally investigated thermal contact resistance of the aluminum honeycomb sandwiched by two aluminum blocks. The example of a tested structure is showed in Fig. 6. It was experimentally observed that effective thermal conductivity in the axial direction of honeycombs is larger than that in the lateral direction and an axial total conductance of honeycombs increases with a decrease of cell size and specimen height.

The friction factor and thermal performance of a heat exchanger having hexagonal fins were tested by Yakut et al. [4]. The effects of hexagonal fins geometry (Fig. 7) and distance between fins on the thermal and pressure drop characteristics were experimentally investigated.

2. Description of the tested heat exchanger

The investigated prototype of the heat exchanger was consisted of twenty identical elements. Each component part, shown in Fig. 8, was composed by eight regular hexagons connected at an angle equal to 109°28′16″ with 20 mm side length. Fig. 9 presents

* Tel.: +48 85 7437912; fax: +48 85 7469576.
E-mail addresses: mzukowski@pb.edu.pl, miroslawzukowski@gmail.com

0017-9310/$ - see front matter © 2008 Elsevier Ltd. All rights reserved.
doi:10.1016/j.ijheatmasstransfer.2008.04.065

Nomenclature

$\dot{C}$	flow-stream capacity rate (W/K)
c_p	fluid specific heat at constant pressure (J/(kg K)
D_H	hydraulic diameter (m)
f_F	Fanning friction factor
F	heat transfer surface area (m^2)
$F(z)$	experimental parameters
$\dot{G}$	mass flow rate (kg/s)
h	convective heat transfer coefficient (W/(m^2 K))
k	thermal conductivity (W/(m K))
L	heat exchanger length (m)
Nu	Nusselt number
P	pressure (Pa)
$\dot{Q}$	heat rate (W)
Re	Reynolds number
U	overall heat transfer coefficient (W/(m^2 K))
v	air velocity (m/s)
$\dot{V}$	volume flow rate (m^3/s)

Greek symbols

Δ	difference between pressure or temperature (Pa or K)
δ	thickness of the heat exchanger separate wall (m)
θ	fluid temperature (K)
ρ	density (kg/m^3)
$\sigma(x)$	uncertainty of variables

Subscripts

a	air
b	brass
C	cold fluid
H	hot fluid
in	inlet boundary
m	measurements
out	outlet boundary

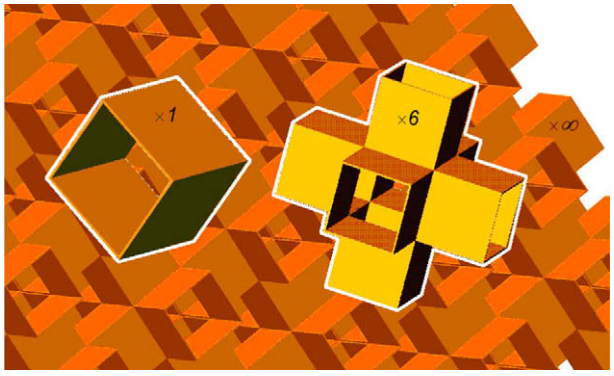

Fig. 1. The first infinite solid.

Fig. 2. The second infinite solid.

the complete heat exchanger which was made of 0.2 mm thickness sheet brass. Before the experimental test the device was insulated with 50 mm thickness polyethylene foam sheets for reducing heat losses from the casing.

Depends on modification inlets and outlets of the base module, the heat exchanger can operates on the cross-, counter-, parallel- or any mixed-flow principles. This is one of the main advantages of the developed construction.

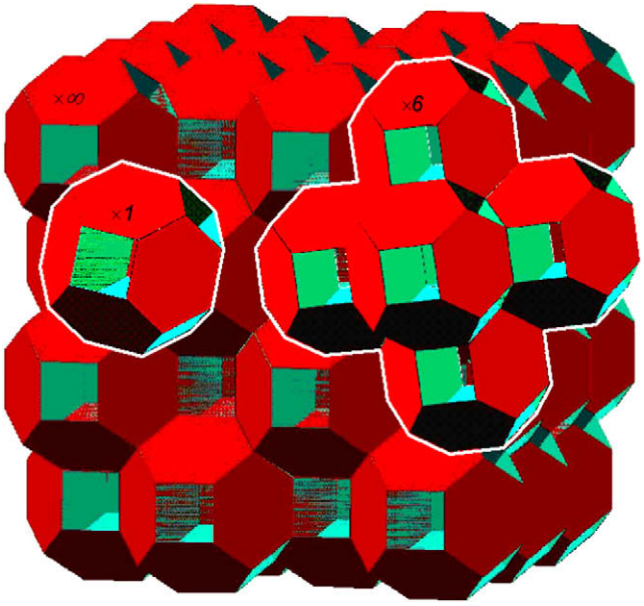

Fig. 3. The third infinite solid.

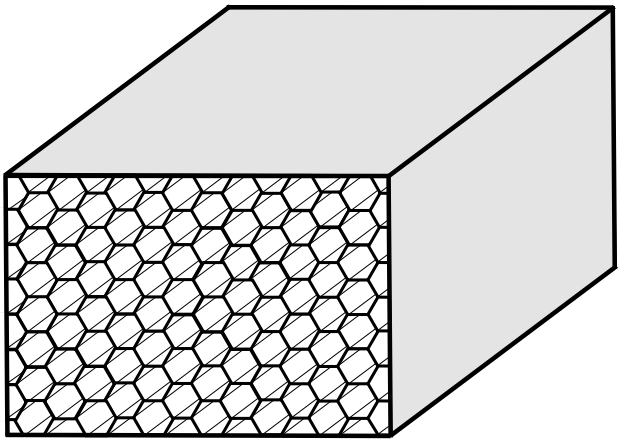

Fig. 4. Heat transfer geometry analyzed in Ref. [1].

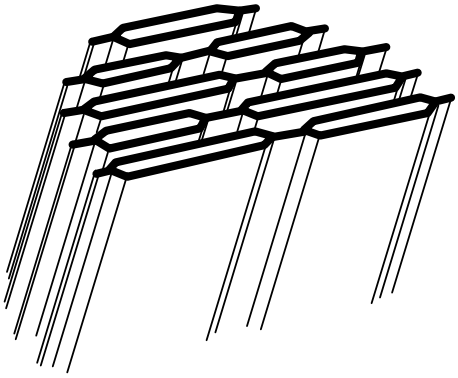

Fig. 5. Double-trapezoidal ducts analyzed by Sadasivam et al.

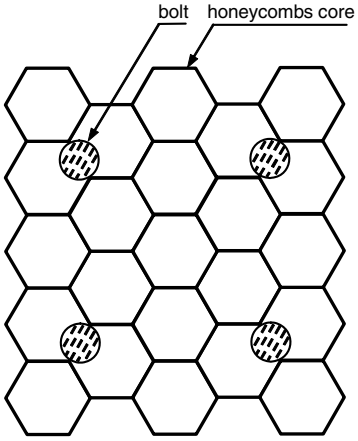

Fig. 6. Geometry of honeycombs with the indication of bolts position.

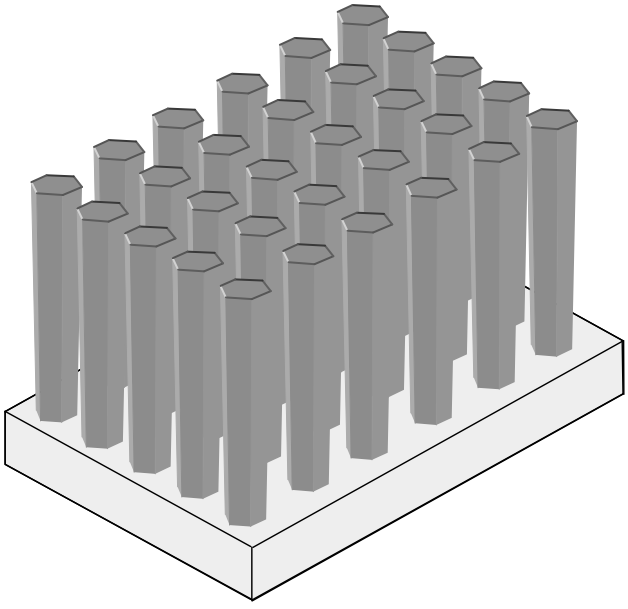

Fig. 7. The arrangement of fins tested by Yakut et al.

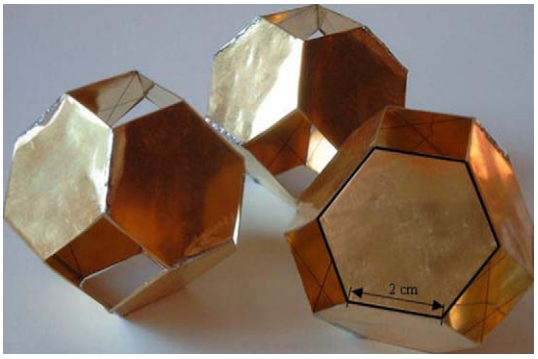

Fig. 8. The basic elements of the heat exchanger.

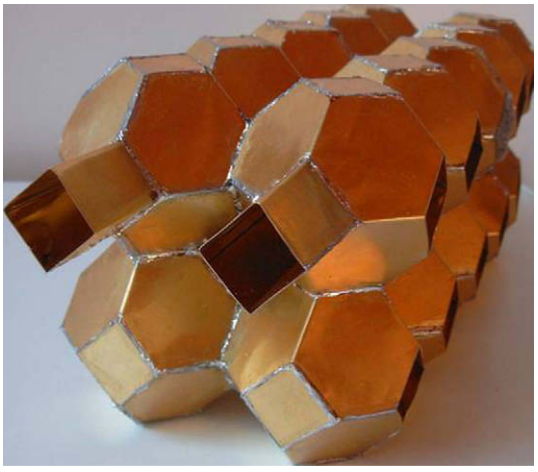

Fig. 9. The investigated prototype of the heat exchanger.

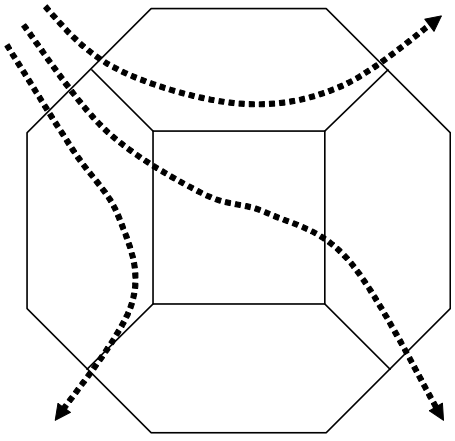

Fig. 10. Fluid flow character in Case 1.

3. Preliminary CFD analysis

The experimental investigations were preceded by a numerical analysis of the heat exchanger thermal performance. The main goal of these simulations was to obtain an influence of the flow domain modification on an intensification of the forced convection heat transfer. It was investigated two cases:

Case 1. – The standard flow geometry without any disturbances, shown in Fig. 10,

Case 2. – Flow disturbance caused by elements in the shape of a cuboid, which are installed perpendicularly to the main flow direction (see Fig. 11).

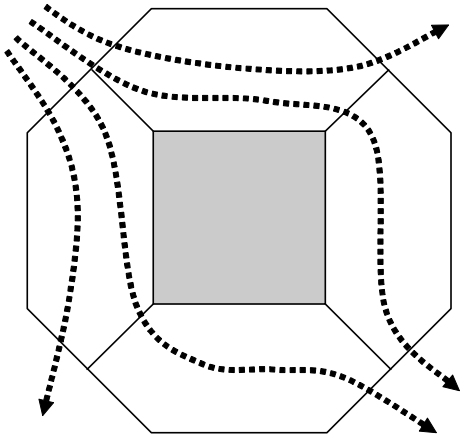

Fig. 11. Fluid flow character in Case 2.

The CFD environment developed by Fluent Inc. (Fluent 6 software package) was used to create computational models of the tested prototype of the heat exchanger. Fluid (air in the current simulation) was assumed to be an incompressible and Newtonian. The two-equation model κ–ε was employed for turbulence modeling. Forced air convection for the air flow domain and conduction heat transfer across the walls were analyzed. On account of a minimal temperature difference of the inside heat exchanger surfaces the long-wave radiation heat transfer was neglected. Gambit preprocessor was used to generate unstructured irregular 3D meshes of the flow domain adapted for requirements of Fluent solver. Figs. 12–14 present the boundary walls geometry of a unitary cell for both simulation variants.

During the simulations a volume flow rate was changed between 2.4 m^3/h and 28.8 m^3/h. It corresponds to Reynolds number ranging from 1000 to 12500. Characteristic dimension (equivalent hydraulic diameter) in Re number was determined for the square inflow area. Velocity fields for the cross-section of the heat exchanger for both cases are shown in Figs. 15 and 16.

We can clearly observe the decrease of air velocity near the separate walls at the first case (Fig. 15). It results in a lower intensity of heat transfer between fluids. As we see in Fig. 16, the turbulent inserts significantly influence on rise of the velocity compare to the previous computational variant.

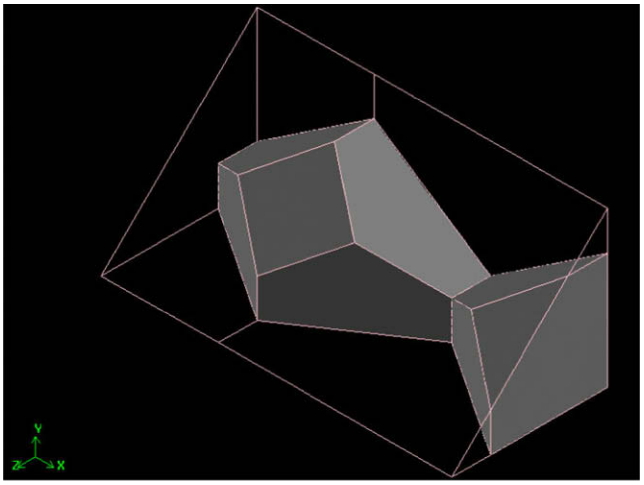

Fig. 12. Flow duct formed between the exchanger plates for the first medium (Case 1).

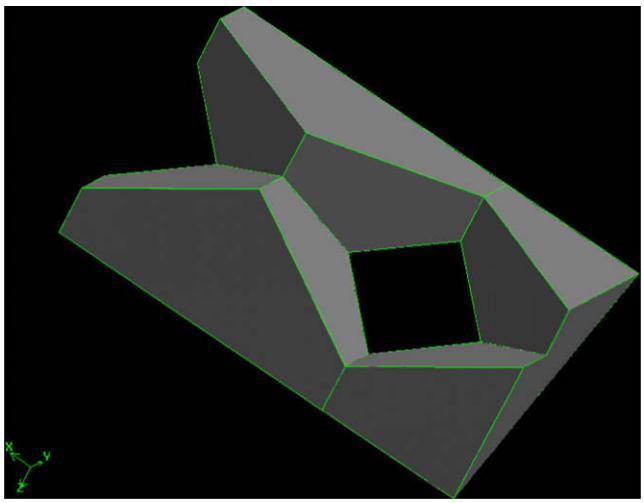

Fig. 13. Flow duct formed between the exchanger plates for the second medium (Case 1).

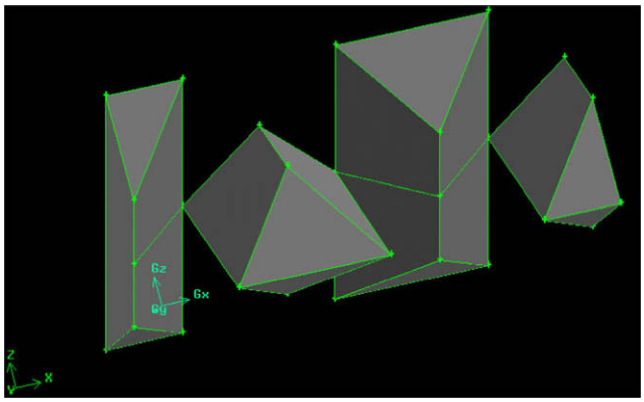

Fig. 14. Turbulence inserts positioned inside the heat exchanger in Case 2.

The distribution of the convective heat transfer coefficient on the heat exchanger walls is presented in Figs. 17 and 18. Both figures show that modification of the flow domain creates a desired effect for the intensification of convective heat transfer and thereby for the extension of heat exchanger efficiency.

In the order to precise explanation the influence of turbulence inserts on a flow disturbance it was prepare two graphs. The first, in Fig. 19, illustrates the dependence of temperature difference between heat exchanger fluids on Nusselt number. The second graph (see Fig. 20) shows relationship between Reynolds number and Nusselt number for both discussed variants.

Based on calculation results we can conclude that:

- The Nusselt number increases about 30% if we use turbulence inserts for the whole range of temperature difference between warmer and colder medium.
- If we increase volumetric flow rate it is observed a linear raise of the difference between Nusselt numbers for Case 2 and Case 1, which ranging from 0% to 32%.

Computational analysis clearly shows that the experimental testing of the just discussed heat exchanger should be realized with include of the flow disturbance elements.

Cuboid turbulence inserts can be used in another way, for example as flow ducts in three or four path flow heat exchangers. We can also obtain a short time thermal energy storage unit by filling these channels with PCM.

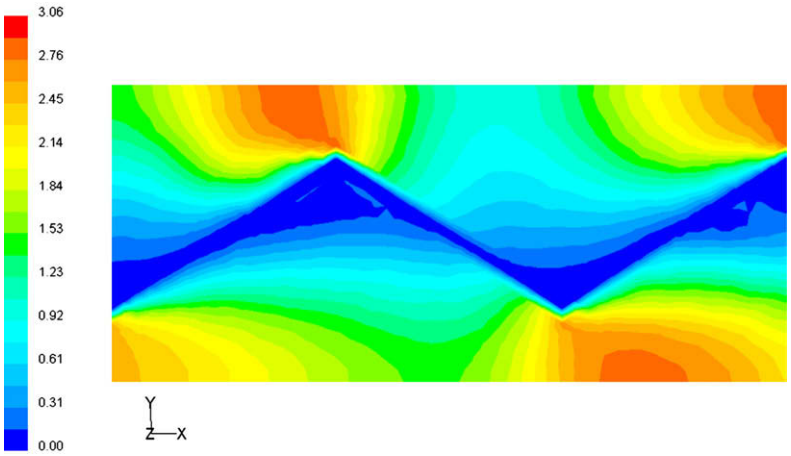

Fig. 15. Contours of velocity magnitude [m/s] for $Re = 3125$ (Case 1).

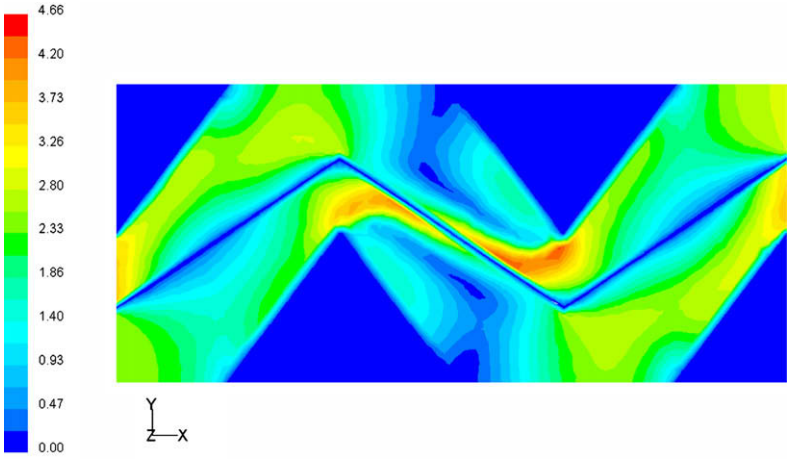

Fig. 16. Contours of velocity magnitude [m/s] for $Re = 3125$ (Case 2).

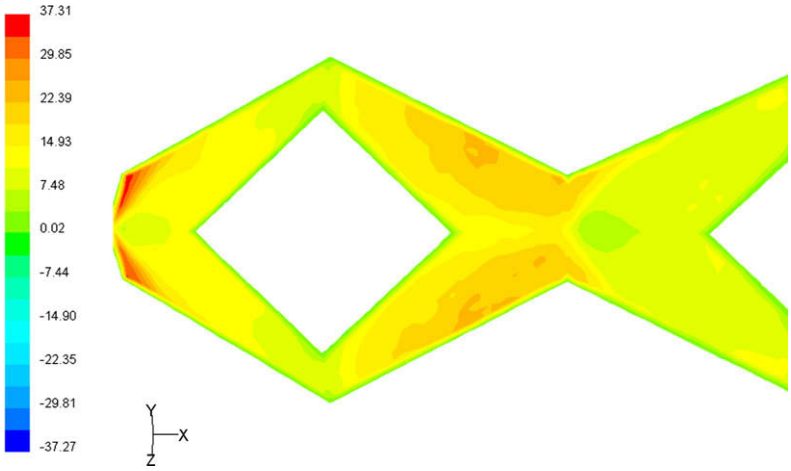

Fig. 17. Contours of surface heat transfer coefficient [$W/m^2 \cdot K$] for $Re = 3125$ (Case 1).

In spite of use of turbulence inserts, we still can find some regions with low convective heat transfer rate. So, the future study should focus on the next modification of the flow domain.

4. Experimental arrangement

The main goals of the experimental investigation were the following:

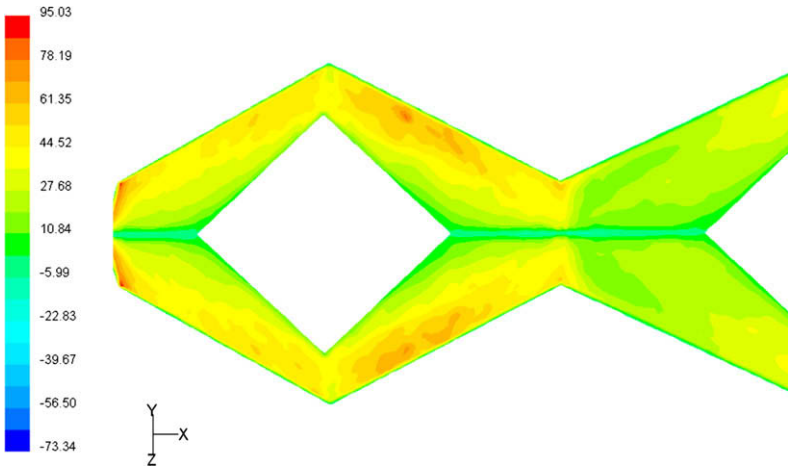

Fig. 18. Contours of surface heat transfer coefficient [W/m^2 K] for Re = 3125 (Case 2).

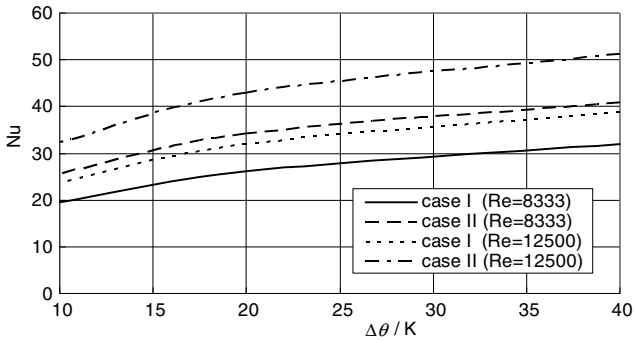

Fig. 19. The dependence of *Nu* number on temperature difference between warmer and colder medium.

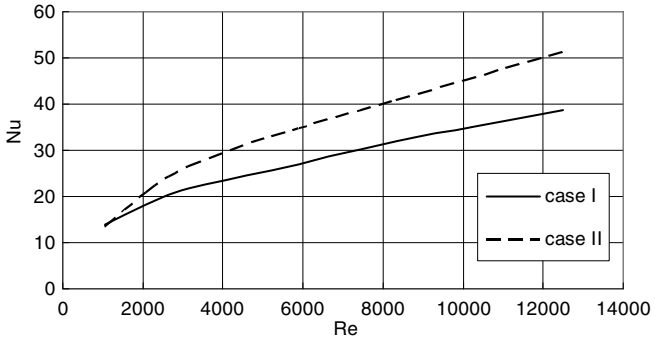

Fig. 20. Nusselt number versus Reynolds number for the both cases.

- Obtained the pressure drop and heat transfer characteristics of the tested device.
- Delivered the essential information, which will be necessary to build the mathematical model of heat and mass transfer inside the heat exchanger.

Schematic arrangement of experimental apparatus is depicted in Fig. 21.

Insulated plastic rectangular ducts were joined in a closed loop for warm air circulation. The air was warm up by an electric resistance heater and value of temperature was regulated by a digital proportional-integral-derivative controller. The temperature sensor of the automatic regulator was placed inside an inlet divider.

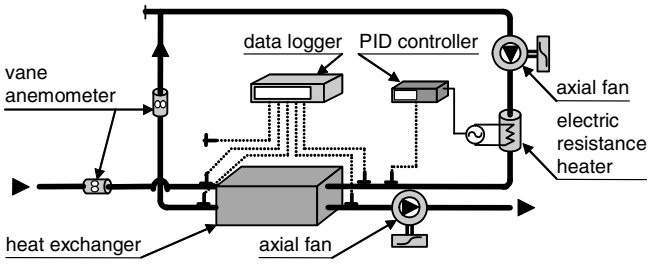

Fig. 21. General arrangement of the experimental setup.

The colder medium was aspirated from the laboratory space and after flowing through the heat exchanger was exhausted from the room.

Volumetric air flow rates were measured by vane anemometers mounted inside plastic channels. The rate flow of the both mediums was changed by an electronic frequency controllers operated with the axial fans. The calibrated resistance sensors Pt100 were used to measure air temperatures inside two inlet headers, two outlet headers and in the laboratory. The experimental results were recorded by a 20-chanall data logger with graphical display and analysis functions for measuring resistance. The pressure drop was measured by an electronic micro-manometer. Static pressure tappings were placed on the inlet and the outlet header.

Experimental analysis was realized for the following range of base parameters changing:

- Air flow rate – from 9.5 m^3/h to 18 m^3/h.
- Temperature of warmer air – 22.5–60.5 °C.
- Temperature of colder air – 13.5–21.5 °C.

Data logger ports were scanned at 5-second intervals and each experimental case was stopped 5 min after the outlet temperature reached a steady state constant value.

In order to indicate the quality of the experimental runs an uncertainty analysis was performed. The error analysis of dependent variables was done by using the root-sum-square approximation given by the following equation:

$$\sigma = \sqrt{\left[\sigma(x_1)\frac{\partial F(z)}{\partial x_1}\right]^2 + \left[\sigma(x_2)\frac{\partial F(z)}{\partial x_2}\right]^2 + \ldots + \left[\sigma(x_3)\frac{\partial F(z)}{\partial x_3}\right]^2}. \quad (1)$$

The uncertainty associated with the dependent variables was determined to be about 5.8% for heat transfer rate $\dot{Q}_m$, 3.5% for Reynolds

number, 4.6% for Nusselt number, and 5.7% for Fanning friction factor f_F.

Instruments error can be estimated on the following level: temperature ±0.3 K, volume flow rate ±0.15 m^3/h and static pressure ±1 Pa.

5. Experimental results and discussion

The main parameters of interest were the Nusselt number and Fanning friction factor. The following procedure was applied for determination of these two parameters.

Firstly, the average heat transfer rate for the developed heat exchanger was calculated by the following relation:

$$\dot{Q}_m = \frac{1}{2}(\dot{V}_H \rho_H c_p \Delta\theta_H + \dot{V}_C \rho_C c_p \Delta\theta_C), \tag{2}$$

where $\Delta\theta_H$ and $\Delta\theta_C$ are temperature changes of hot and cold fluids.

In above equation air temperatures and flow rates were directly measured. Air leakage through the ductwork was neglected in the present study. Fig. 22 shows the total heat transfer rate, calculated from Eq. (2), as a function of Reynolds number and temperature changes of mediums.

During 66 experimental tests the heat transfer rate was varied from 16 W to about 170 W. It should be noted that low value of $\dot{Q}_m$ was resulted from: firstly, a small dimensions of the heat exchanger and secondly, low air flow rate.

An intensity of convective heat transfer can be expressed by Nusselt number, which is given by Eq. (3).

$$\overline{Nu} = \frac{\overline{h}_a D_h}{k_a}. \tag{3}$$

In order to determine of convective heat transfer coefficient $\overline{h}_a$ in Eq. (3) we should apply the following two relations:

$$\frac{1}{\overline{\overline{U}}} = \frac{1}{\overline{h}_{a,C}} + \frac{\delta}{k_b} + \frac{1}{\overline{h}_{a,H}}, \tag{4}$$

$$\overline{U} = \frac{\dot{Q}_m \ln\left(\frac{\Delta\theta_{in}}{\Delta\theta_{out}}\right)}{F(\Delta\theta_{in} - \Delta\theta_{out})}, \tag{5}$$

where: $\Delta\theta_{in}$ and $\Delta\theta_{out}$ represent temperature difference between two air flows on inlet and outlet boundary of the examined device.

We can assume that convective heat transfer coefficients on the both sides of the heat exchanger separate wall, $\overline{h}_{a,C}$ and $\overline{h}_{a,H}$, have the same value. Thus,

$$\overline{h}_a = \left[\frac{2F(\Delta\theta_{in} - \Delta\theta_{out})}{\dot{Q}_m \ln\left(\frac{\Delta\theta_{in}}{\Delta\theta_{out}}\right)} + \frac{2\delta}{k_b}\right]^{-1}. \tag{6}$$

For the special case of the same heat capacity of both medium flows

$$\dot{C}_H = \dot{C}_C, \tag{7}$$

where $\dot{C} = \dot{G}c_p$, the convective heat transfer coefficient should be calculated from the other following relation:

$$\overline{h}_a = \left[\frac{2F\Delta\theta_H}{\dot{Q}_m} + \frac{2\delta}{k_b}\right]^{-1} \text{ or} \tag{8}$$

$$\overline{h}_a = \left[\frac{2F\Delta\theta_C}{\dot{Q}_m} + \frac{2\delta}{k_b}\right]^{-1}. \tag{9}$$

The logarithmic scale for Re number was selected to show heat transfer characteristic of the tested device (Fig. 23).

The experimental results can be approximated by a power function of Reynolds number (Eq. (10)) for the constant value of Prandtl number equal to 0.701.

$$Nu = 0.041 Re^{0.801}. \tag{10}$$

It can be concluded that tested flow geometry provides a sufficient intensity of heat transfer by forced convection. However, for increasing heat exchange efficiency the fins should be installed.

One of the important features of any heat exchanger should be a low level of pressure drop at the operating conditions. The static pressure difference measured between inlet and outlet of the device is presented in Fig. 24.

As expected, the experimental test showed that prototype of the heat exchanger is characterized by a low value of pressure losses. This feature is a result of no fins and corrugated surfaces.

In the present study Fanning friction factor f_F was obtained, too. The heat exchanger core friction characteristic, described by f_F, is expressed as

$$f_F = \frac{1}{4}\frac{\left(\frac{\Delta p}{L}\right) D_H}{\frac{1}{2}\rho_a (\bar{v})^2}. \tag{11}$$

Fig. 25 presents the dependence of Fanning friction factor on Reynolds number. A solid line on the chart approximates the experimental data.

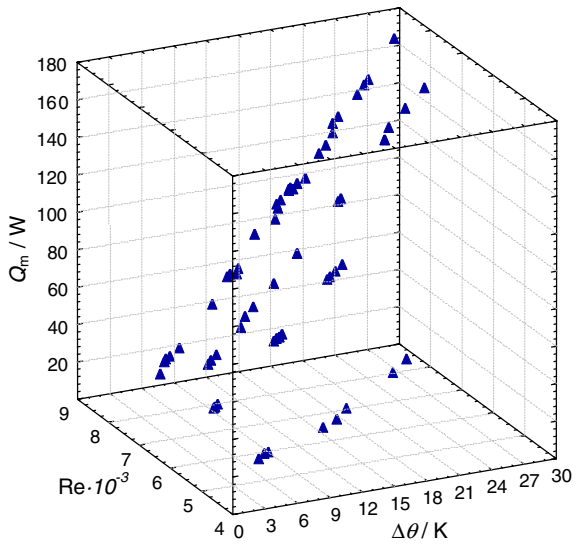

Fig. 22. Dependence of the heat transfer rate of heat exchanger on *Re* number and on difference between average inlet and outlet air temperature.

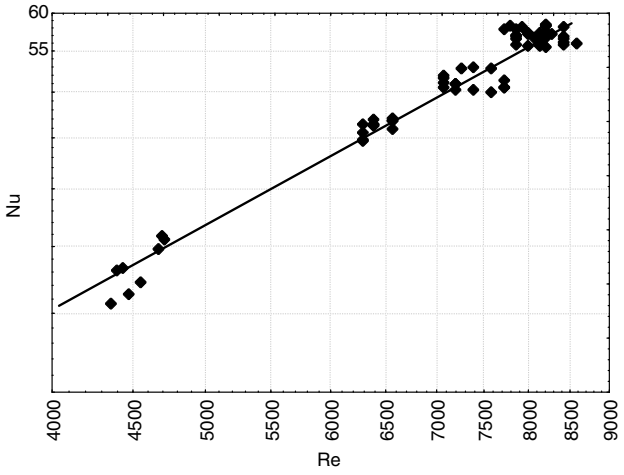

Fig. 23. The Nusselt number as a function of Redynolds number.

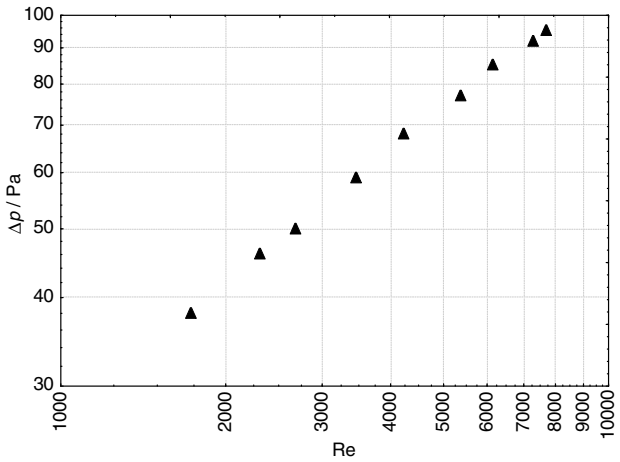

Fig. 24. Air pressure drop versus Reynolds number.

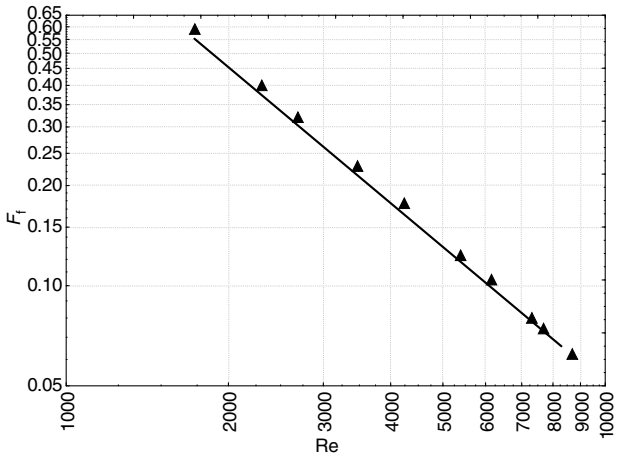

Fig. 25. Friction factor characteristic of turbulent air flow.

The results of f_F calculation can be approximately described by the following equation:

$$f_F = 744Re^{-1.99}. \quad (12)$$

6. Summary and concluding remarks

The main goal of this paper is presentation of the possibility of infinite regular polyhedrons utilization in heat exchanger construction. The study of the heat transfer and pressure drop characteristic of the labyrinth heat exchanger was carried out. The experimental and calculation results show that the core of the tested prototype has the following features: low pressure losses and sufficient intensity of convection heat transfer. Additionally, described construction allows to free arrangement of flow paths or to use of PCM for increasing thermal capacity of the device. Reported here study has been focused primarily on the simplest construction based on geometry of polyhedrons and this is the first stage of the project.

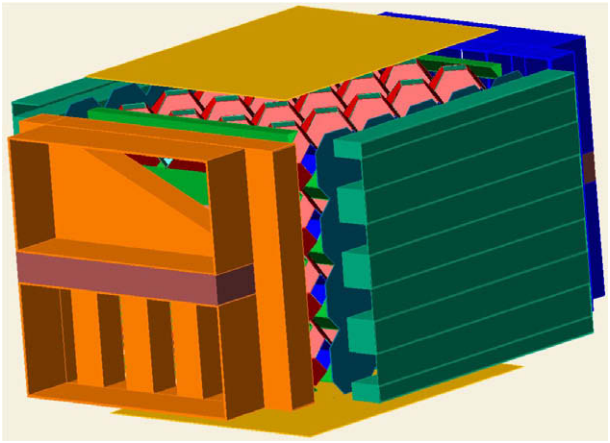

Fig. 26. Heat exchanger with flow recirculation mode inside the core.

The future work will aim at improvement of the efficiency by an increasing of a heat exchange surface area and by a modification of fluid flow passes. A preliminary design of four rows heat exchanger with utilization of turbulence inserts as additional flow ducts for recirculation of fluids is shown in Fig. 26.

Besides, the results of the present work will be used to validity the new method for designing of heat exchangers with labyrinth flow domain.

Acknowledgements

This investigation was carried out under a computational grant of the Polish Ministry of Scientific Research and Information Technology MNiSW/Sun6800/PBiałystok/027/2007 and Grants of Bialystok Technical University: No. S/WBiIS/23/08 and No. W/WBiIS/42/2006.

References

[1] T.J. Lu, Heat transfer efficiency of metal honeycombs, Int. J. Heat Mass Transfer 42 (1999) 2031–2040.
[2] R. Sadasivam, R.M. Manglik, M.A. Jog, Fully developed forced convection through trapezoidal and hexagonal ducts, Int. J. Heat Mass Transfer 42 (1999) 4321–4331.
[3] C.L. Yeh, Y.F. Chen, C.Y. Wen, K.T. Li, Measurement of thermal contact resistance of aluminum honeycombs, Exp. Therm. Fluid Sci. 27 (2003) 271–281.
[4] K. Yakut, N. Alemdaroglu, B. Sahin, C. Celik, Optimum design-parameters of a heat exchanger having hexagonal fins, Appl. Energy 83 (2006) 82–98.